Catalysis Today 154 (2010) 21–30

Contents lists available at ScienceDirect

Catalysis Today

journal homepage: www.elsevier.com/locate/cattod

Gold nanoparticles on ceria supports for the oxidation of carbon monoxide

S.A.C. Carabineiro [a,*], A.M.T. Silva [a], G. Dražić [b], P.B. Tavares [c], J.L. Figueiredo [a]

[a] Universidade do Porto, Faculdade de Engenharia, LSRE/LCM – Laboratório Associado, Rua Dr. Roberto Frias s/n, 4200-465 Porto, Portugal
[b] Jozef Stefan Institute, Department of Nanostructured Materials, Jamova 39, SI-1000 Ljubljana, Slovenia
[c] Universidade de Trás-os-Montes e Alto Douro, CQVR Centro de Química – Vila Real, Departamento de Química, 5001-911 Vila Real, Portugal

ARTICLE INFO

Article history:
Available online 12 February 2010

Keywords:
Gold
Ceria
Nanoparticles
Carbon monoxide
Oxidation

ABSTRACT

Ultrafine cubic CeO_2 particles were prepared by a solvothermal method, using methanol and different conditions of synthesis, and compared with a commercial CeO_2, used as received and after a thermal treatment in nitrogen. The solvothermally prepared materials showed higher specific surface areas (from ~124 to ~157 m^2/g) than the commercial sample (~20 m^2/g). Au was loaded onto the obtained ceria supports by a double impregnation (DIM) method. Samples were characterised by high-resolution transmission electron microscopy (HTREM), selected area electron diffraction (SAED), energy-dispersive X-ray spectrometry (EDXS), high-angle annular dark-field imaging (HAADF), X-ray diffraction (XRD), X-ray photoelectron spectroscopy (XPS), temperature programmed reduction (TPR) and temperature programmed desorption (TPD). Activities for CO oxidation were compared and results were discussed. A gold reference catalyst from the World Gold Council (Type C—Au/Fe_2O_3) was also used for comparison purposes. Considering the ceria supports alone, the solvothermally prepared samples clearly showed better performance for CO oxidation than the commercial ceria. This can be due to their large amounts of surface oxygen groups, as seen by TPR and TPD, since XRD showed that the same phase was present in all ceria samples. When gold was loaded, full CO conversion was obtained at much lower temperatures. The best results were obtained with the commercial as received sample, which can be explained by the small size of the Au particles (2–5 nm). Other samples (solvothermal) yielded larger Au particle sizes (~10–30 nm). Although the gold particle size of these solvothermal materials is far from the "ideal" range (below 5 nm), and their activity is consequently lower than that of the commercial ceria, these samples still show better catalytic behaviour in comparison to the reference catalyst. It was shown that Au was in its metallic state when supported in the commercial ceria sample, while a larger contribution from oxidic Au was found in the solvothermal samples.

1. Introduction

The oxidation of carbon monoxide is a reaction of outstanding importance in pollution control (CO removal), fuel-cells, and gas sensing. Although simple and intensively studied, this reaction is still poorly understood and its mechanistic pathways are still uncertain. At the time of the early work of Haruta in the 1980s, the activity for gold-supported catalysts came as a surprise [1,2] but it is now well known that gold-supported nanocatalysts are effective for CO oxidation at very low temperatures. Activities do, however, depend on choice of metal oxide support. Significant progress has been made ever since, and a number of reviews are written (e.g. [3–11]).

Gold on ceria (CeO_2) has proved to be a very effective catalyst for this reaction [9–23] and for other fuel-cell/automotive important reactions, such as water-gas shift (WGS) [9–11,24–32] and preferential oxidation of CO in the presence of hydrogen (PROX) [9–11,33–36]. These results are of particular interest, since ceria is extensively employed in automotive three-way emission-control catalysts, due to its capacity to undergo a rapid change in oxidation state upon changes in the redox potential of the exhaust gases [9–11].

Nanocrystalline CeO_2 samples are expected to present superior physical properties. Some related results have been obtained for them, such as blue-shift in the UV absorption spectra, lattice expansion, Raman-allowed modes shifting and broadening, four orders of magnitude increase in the electronic conductivity and pressure-induced phase transformation, which are partially attributed to the quantum size effect and surface effect [37–39]. In fact, it has been shown that the activity for CO oxidation could be enhanced by two orders of magnitude when depositing gold nanoparticles on mesoporous CeO_2 nanocrystals, comparing with the regular supported ceria samples, or those prepared by coprecipitation [12]. Also, the preparation and characterisation

* Corresponding author. Tel.: +351 225081582; fax: +351 225081449.
E-mail address: sonia.carabineiro@fe.up.pt (S.A.C. Carabineiro).

0920-5861/$ – see front matter © 2010 Elsevier B.V. All rights reserved.
doi:10.1016/j.cattod.2010.01.036

of nanosized CeO_2 samples attracted great interest for their improved properties. Zhou et al. studied optical and catalytic performances of CeO_2 nanocrystals [37]. Nanowires, nanorods and nanotubes of CeO_2 were produced and their large-scale syntheses were also performed [14,40–42]. Recently, uniform-sized CeO_2 nanocrystals with porous structures were used as supports, and Au–CeO_2 nanocomposite catalysts showed high catalytic activity in the reaction of CO oxidation [20].

It has been shown that hydrothermal oxidation is a useful preparation method for ceria nanoparticles with different shapes [43,44]. When a solvent other than water is used, the process is usually known as solvothermolysis [45–47]. Concerning Au deposition, a careful preparation procedure is crucial in order to obtain nanoparticles well dispersed on the support. The crystalline form of the support, the gold particle size and the metal support interaction all play a role in the activity, and are determined by the details of the preparation method [3–11].

In this work, we used a solvothermal method for preparing the ceria supports, which is an interesting approach for the synthesis of nanostructured catalysts, already published in a previous paper from our group [48]. We also wanted to combine this procedure with a less usual Au loading method, such as double impregnation (DIM) [49], in order to prepare Au nanoparticles. To the best of our knowledge, the only report on the use of DIM is the work of Bowker et al. dealing with TiO_2 samples [49]. These authors proposed that this method represents an environmentally and economically more favorable route to high activity gold catalyst production, when compared with the traditional deposition–precipitation (DP) method [49]. Moreover, the majority of the gold catalysts referred in the literature typically contain 2–10 wt.% Au and less studies deal with a lower loading of 1 wt.%. Au [9–11].

In the present work, 1 wt.%. Au/ceria materials were prepared by the combination of the solvothermal method for CeO_2 synthesis and the DIM method for Au loading. These catalysts were tested in the oxidation of CO. A commercial ceria sample and a Au/Fe_2O_3 gold reference catalyst, supplied by the World Gold Council (WGC) [50], were also used for comparison purposes.

2. Experimental

2.1. Catalysts preparation

2.1.1. CeO_2 materials

Ultrafine shaped CeO_2 particles were prepared by the solvothermal method, as described in a previous publication [48]: the cerium(III) precursor was slowly dissolved in 75 ml of methanol in a 160 ml 316-SS high pressure autoclave (Parr Instruments, USA, Mod. 4564) equipped with a temperature controller (Mod. 4842), under continuous stirring in order to obtain an equimolar solution with a metal concentration of 0.10 M, which was prepared in alkaline conditions using KOH (3 M). The solution obtained was transferred to a Teflon vessel inserted in the autoclave and heated up to the desired temperature (150 °C) under autogenous pressure. The solution was then maintained at the desired temperature for a duration of 150 min under a continuous stirring speed of 500 rpm. At the end of this stirring period, the autoclave was cooled to room temperature. Different conditions of synthesis were investigated: $pK_a = 8.5$ at $T = 120$, 150 and 220 °C, and $pK_a = 26.5$ at $T = 150$ °C. These materials were continuously washed in up-flow mode with deionized water (ca. 3 ml/min) for several hours with the aid of a peristaltic pump, dried in an oven overnight at 120 °C and used as prepared (since it was shown that a similar behaviour was observed with and without calcination, as discussed above). A commercial CeO_2 (Fluka) was also used for comparison, as received, and treated during 2 h at 400 °C in N_2.

2.1.2. Au/CeO_2 materials

Au was loaded on the ceria supports by the double impregnation method (DIM) [49], using $HAuCl_4{\cdot}3H_2O$ as the gold precursor (Alfa Aesar), in order to achieve 1 wt.%. content of Au. Briefly, this method consists in impregnating the support with an aqueous solution of the gold precursor and then with a solution of Na_2CO_3, under constant ultrasonic stirring, followed by washing with water and drying in an oven overnight at 120 °C. The advantage of this method is that it removes chloride, which is known to cause sintering of Au particles, thus turning them inactive [9–11].

2.2. Characterisation techniques

The ceria materials were analysed by adsorption of N_2 at −196 °C, in a Quantachrom NOVA 4200e apparatus.

Temperature programmed reduction (TPR) and temperature programmed desorption (TPD) experiments were performed in a fully automated AMI-200 Catalyst Characterization Instrument (Altamira Instruments), equipped with a quadrupole mass spectrometer (Dymaxion 200 amu, Ametek). In a typical TPR experiment, ∼50 mg of sample was placed in a U-shaped quartz tube located inside an electrical furnace and subjected to a 10 °C/min heating rate up to 1100 °C, under He flow of 29 cm^3/min and H_2 flow of 1.5 cm^3/min. For TPD experiments, similar conditions were employed (but no H_2 was used).

A JEOL 2010F analytical electron microscope, equipped with a field-emission gun was used for high-resolution transmission electron microscopy (HRTEM) investigations. The microscope was operated at 200 kV, and an energy-dispersive X-ray spectrometer (EDXS) LINK ISIS-300 from Oxford Instruments with a UTW Si–Li detector employed for the chemical analysis. The samples for TEM were prepared from a diluted suspension of nanoparticles in ethanol. A drop of suspension was placed on lacey carbon coated Ni grid and allowed to dry in air. *Z*-contrast images were collected using a high-angle annular dark-field (HAADF) detector, in scanning transmission mode (STEM).

X-ray diffraction (XRD) analysis was carried out in a PAN'alytical X'Pert MPD equipped with a X'Celerator detector and secondary monochromator (Cu Kα, $\lambda = 0.154$ nm, 50 kV, 40 mA; data recorded at a 0.017° step size, 100 s/step). Rietveld refinement with PowderCell software [51] was used to identify the crystallographic phases present and to calculate the crystallite size from the XRD diffraction patterns. This method employs a modified version of the Debye–Scherrer equation to simultaneously determine the crystallite size and non-uniform strain (the model can be found in Ref. [52]).

X-ray photoelectron spectroscopy (XPS) analyses were performed with a VG Scientific ESCALAB 200A spectrometer using Al Kα radiation (1486.6 eV). Charging effects were corrected by adjusting the binding energy of C 1s to 284.6 eV. Regarding this last technique, the relative area of the Ce 3d peak at ca. 917 eV (u''', as defined in Fig. 3), characteristic of CeO_2 (since it is absent in pure Ce_2O_3) was used for semi-quantitative estimation of the relative amount of cerium present as Ce(IV), according to the relationship reported by Shyu et al. [53].

2.3. Catalytic tests

Catalytic activity measurements for CO oxidation were performed using a continuous-flow reactor. The catalyst sample (200 mg) was placed on a quartz (silica) wool plug in a 45 cm long silica tube with 2.7 cm i.d., inserted into a vertical furnace equipped with a temperature controller. Reactant gas (5% CO, 10% O_2 in He) was passed through the catalytic bed at a total flow rate of 50 ml/min. A gold reference catalyst (Type C—Au/Fe_2O_3) was supplied by the WGC [50] and used for comparison purposes.

As this catalyst contained 5 wt.%. Au (and our ceria samples had 1 wt.%. Au), 40 mg mass of this reference material was used in order to have the same amount of Au present, as with the ceria materials. This experiment with the WGC catalyst was also performed using 40 mg catalyst mixed with 0.16 g of an inert (Carborundum, CSi, from VWR), in order to have the same mass as the experiments with ceria and the results were very similar. The flow rates were controlled by mass flow controllers and gases were supplied by specialised companies (Praxair, Air Liquide). The reaction temperature was raised from room temperature until full conversion was obtained by steps of 25 °C. The reactor was maintained at each temperature for 20 min in order to obtain experimental values at steady state. The composition of the outgoing gas stream was determined at the exit of the tube using a gas chromatograph equipped with a capillary column (Carboxen 1010 Plot, Supelco) and a thermal conductivity detector (Valco Instruments Co. Inc.).

3. Results and discussion

3.1. Characterisation of CeO_2 samples

3.1.1. BET surface area

Table 1 shows the characterisation results for the ceria samples obtained by N_2 adsorption at −196 °C. As expected, a higher temperature of solvothermal preparation (from 120 to 220 °C, at the same pK_a) causes a slight decrease in the specific surface area (from 153 to 124 m^2/g). This is in agreement with the results reported by Demazeau and co-workers, in which samples prepared also by solvothermolysis (using ethanol as solvent) showed a decrease in the surface area (from 79 to 33 m^2/g) with increasing temperature of synthesis (from 200 to 350 °C) [45]. An increase in the pK_a (from 8.5 to 26.5) at the same temperature (150 °C) causes a moderate increase in the surface area (from 138 to 157 m^2/g). Corma and co-workers obtained a value of 180 m^2/g for a nanocrystalline ceria support prepared by thermolysis [12], which is higher than the value obtained in this work for the sample prepared at pK_a = 26.5, 150 °C. A value of 198 m^2/g was reported for mesoporous CeO_2 prepared using silica templates [54]. Boccuzzi and co-workers [55] used a CeO_2 support (prepared from an aqueous solution of $Ce(NO_3)_3$ by precipitation followed by calcination in air at 400 °C for 4 h, according to a method described by Haruta and co-workers [56]) that had a surface area of 118 m^2/g. Similar values of 140 and 121 m^2/g were obtained, respectively, by Flytzani-Stephanopoulos and co-workers [27] and Davis and co-workers [29] for ceria supports also prepared by precipitation of the nitrate (with urea). 105 m^2/g was the reported value for a CeO_2 sample obtained by a sol–gel process [20], while direct calcination of cerium acetylacetonate [$Ce(C_5H_7O_2)_3$], at 400 °C, for 2 h, gave a support with 115 m^2/g [19]. Precipitation of the former with ammonia and K_2CO_3 led to lower surface areas of 85 m^2/g [17] and 70 m^2/g [36], respectively, which are smaller than those of our samples. Andreeva et al. [24] obtained a value of 84 m^2/g for a ceria prepared also from the precipitation of the nitrate precursor, while Flytzani-Stephanopoulos and co-workers [25] obtained 79 m^2/g for a ceria prepared by urea gelation/coprecipitation. On the other hand, surface areas from 100 to 114 m^2/g were obtained for the uncalcined mesoporous ceria, while the calcined materials, showed surface areas ranging from 54 to 74 m^2/g [31]. A surface area of 44 m^2/g was reported for ceria prepared by combustion [34], while 53 m^2/g was reported for CeO_2 (fluorite) prepared by the calcination of the nitrate at 973 K for 2 h [57]. CeO_2 prepared by supercritical antisolvent precipitation gave materials with 31 m^2/g [19]. A commercial ceria support from Alfa Aesar revealed a lower area of 32 m^2/g [16], not very different from the value obtained for the commercial sample from Fluka used in this work (20 m^2/g). A thermal treatment on this commercial support causes a slight decrease in the surface area (17 m^2/g). Other authors also reported a decrease in the surface area by thermally treating a CeO_2 support with increasing temperatures [17,25,28,30].

Table 1
BET surface areas (m^2/g) of ceria samples obtained by the adsorption of N_2 at 77 K, and crystallite sizes obtained by XRD.

Ceria sample	BET area (m^2/g)	Ceria crystallite size (nm)
Solvothermal, pK_a = 8.5, 120 °C	153	4.8
Solvothermal, pK_a = 8.5, 150 °C	138	5.7
Solvothermal, pK_a = 8.5, 220 °C	124	7.5
Solvothermal, pK_a = 26.5, 150 °C	157	4.6
Commercial	20	54
Commercial thermally treated	17	53

3.1.2. XRD

In all cases, cerianite CeO_2, with face-centered cubic (*Fm-3m*) fluorite structure, was the only phase detected [ref. JCPDS 03-065-5923] by XRD (Fig. 1a). The same fluorite structure was reported in hydrothermally prepared ceria nanoparticles [58], in ceria nanorods obtained from the reaction of metallic cerium with HCl and later with KOH [14], in ceria supports prepared by the precipitation of the nitrate (with urea [25,27] and with ammonia [17]), in mesoporous ceria [31], and for a commercial ceria support from Alfa Aesar [16]. Corma and co-workers found cerianite CeO_2, but traces of monoclinic Ce_6O_{11} were also detected [12].

The crystallite sizes of solvothermal samples, obtained by XRD, are also displayed in Table 1. The values range from 4.6 to 7.5 nm, depending on the preparation conditions. An increase in the pK_a (from 8.5 to 26.5, at 150 °C) causes a decrease in the crystallite size from 5.7 to 4.6 nm (which agrees well with the observed increase in the surface area from 138 to 157 m^2/g). With increasing temperature of synthesis (from 120 to 220 °C, at pK_a = 8.5), the particle size increases (which agrees well with the decrease in the surface area from 153 to 124 m^2/g). In general, the values obtained are comparable to those reported for CeO_2 particles also prepared by solvothermolysis using methanol as solvent (∼3 nm as determined by SAED) [46], to those of CeO_2 prepared by supercritical antisolvent precipitation (3–8 nm) [19], and to the 6 nm size found for ceria derived from a commercial colloidal solution of cerium acetate [22]. They are also similar to the 3–6 nm range reported by Boccuzzi and co-workers [55], to the value of 6.6–7.1 nm obtained by Flytzani-Stephanopoulos and co-workers [25], and to the value of 7 nm obtained by Manzoli et al. [36], all of them prepared by the precipitation of cerium nitrate. They are, however, much smaller than those previously reported for traditionally precipitated CeO_2 (15.9 nm) [59], hydrothermal ceria nanoparticles (15.5 nm) [58], mesoporous ceria (8.9–11.4 nm) [31] and combustion prepared ceria (11 nm) [34].

When compared with the solvothermal samples, the commercial supports used in this work have XRD peaks significantly narrower and with higher intensities (Fig. 1a), characteristic of larger crystallites (∼53 nm) and higher degree of crystallinity. The crystallite size of the commercial treated sample is not much different from the untreated sample. These values are comparable to the 46 nm reported for a commercial CeO_2 from Daiichi [21].

The remarkable correlation of the BET area values and the crystallite particle sizes found in Table 1 made us wonder if they obey to a theoretical relationship between the two. We calculated the dependence for spherical, cubic and hexagonal prismatic shapes, using the density (ρ) value of 7.204×10^6 g/m^3 for CeO_2. The relationship for spherical and cubic shape particles is:

$$A_{BET} = \frac{6}{\rho t_c}$$

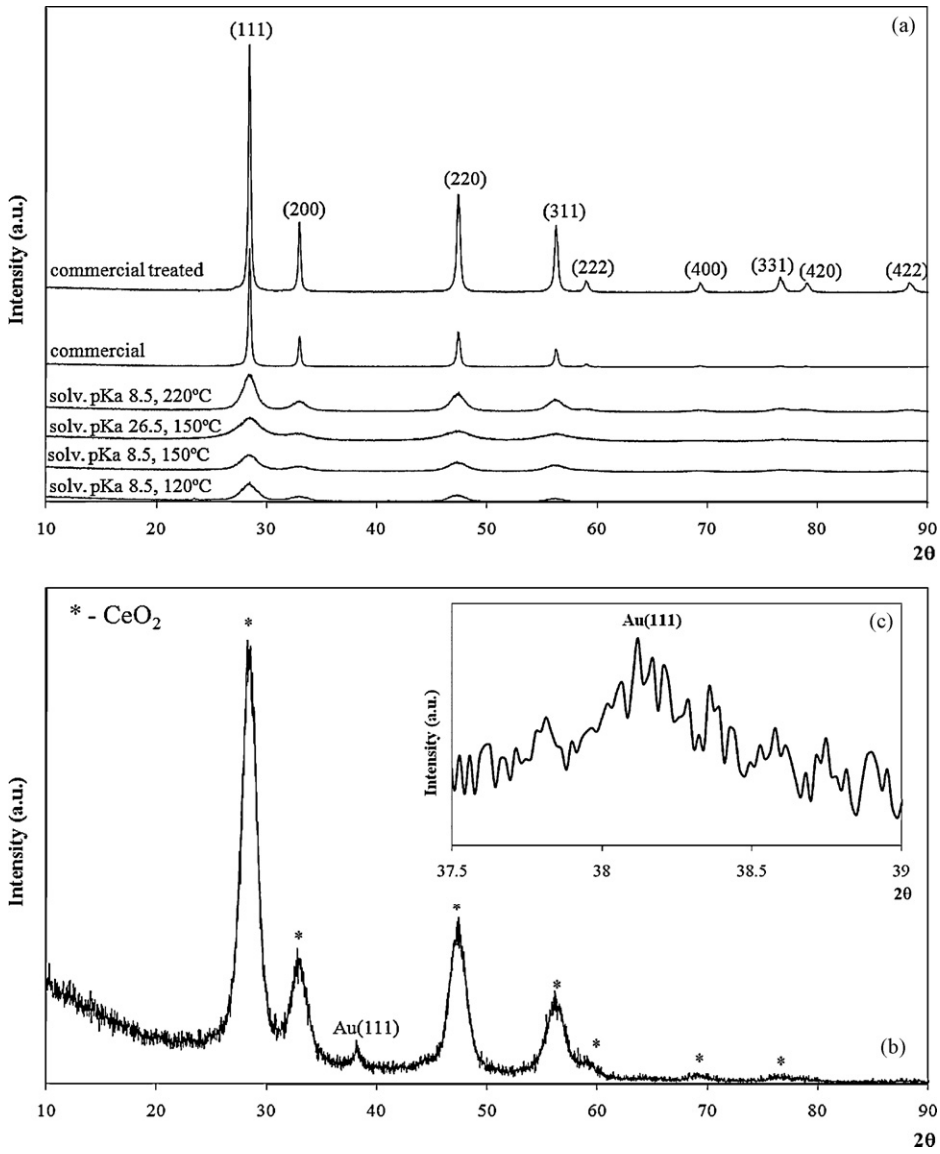

Fig. 1. XRD spectra of the solvothermal and commercial CeO_2 samples (a) and of the solvothermal CeO_2 sample prepared at pK_a = 8.5, T = 120 °C with 1% Au (b) with a detail of the Au(1 1 1) peak (c) as an inset.

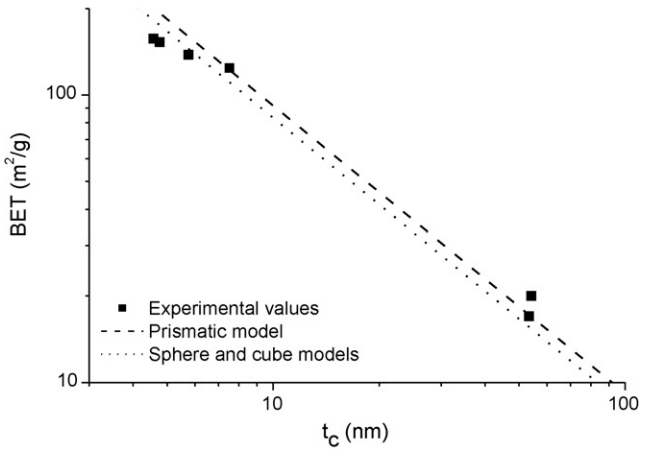

Fig. 2. Correlation between BET surface area (m^2/g) and crystallite size (nm) for CeO_2 samples.

The relationship considering hexagonal prismatic particles (with height and base dimensions equal to t_c) is:

$$A_{BET} = \frac{6.62}{\rho t_c}$$

where A_{BET} is the BET surface area (m^2/g) and t_c is the size of ceria crystallites (m). It can be seen in Fig. 2 that these models match very well with the experimental results (although there is a slight deviation from linearity for crystallites smaller than 10 nm, explained by particle superposition). It also agrees with the XRD results that showed a cubic structure for ceria and with the TEM results of Fig. 3.

Regarding the Au/ceria samples, only some traces of gold were detected by XRD (one example is shown in Fig. 1b and c), and the Au *Fm-3m* cubic form was identified; however, it was not possible to determine accurately the gold particle size, most likely because the loading was too low for an efficient analysis of the peaks. The CeO_2 crystallite sizes of the commercial sample decreased from 54 to 42 nm when Au was added, while the solvothermal samples showed practically no change. A decrease in the ceria particle size upon loading with Au was also reported by Manzoli et al. [36]. In

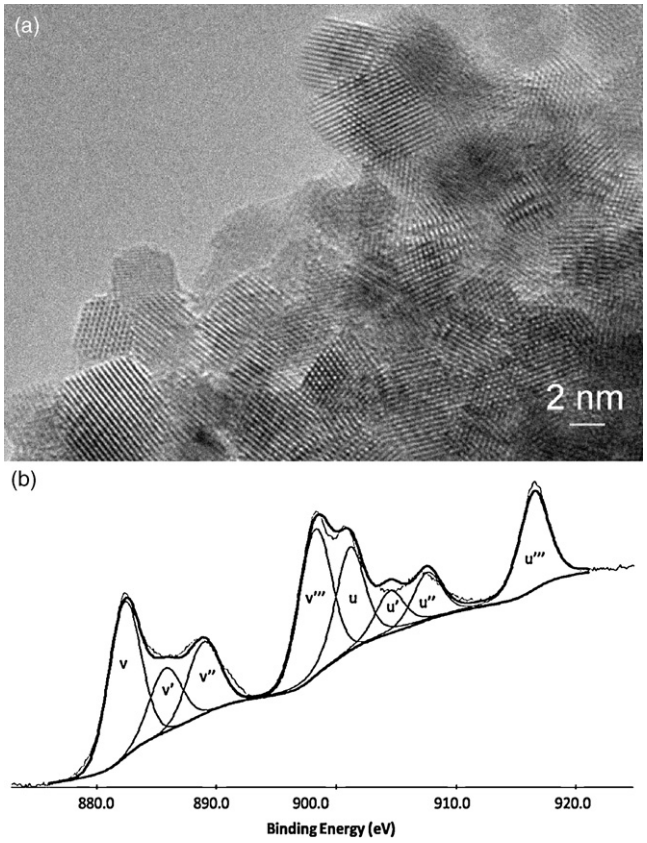

Fig. 3. HRTEM image (a) and Ce 3d XPS spectrum with peak deconvolution (b) of CeO_2 sample prepared at $pK_a = 8.5$, $T = 120\ ^\circ C$.

addition, XRD results did not show any presence of chloride or sodium on the samples.

3.1.3. HRTEM/HAADF/EDXS

Ceria only and Au/ceria samples were analysed by HRTEM/HAADF/EDXS. Fig. 3a displays a HRTEM image of the CeO_2 sample prepared solvothermally at $pK_a = 8.5$, $T = 120\ ^\circ C$, as a representative example of the supports prepared by this procedure. The appearance is that of ultrafine agglomerated crystallites, with a body diagonal of ~3–8 nm, which correlates very well with XRD and BET results. These nanoparticles of ceria have different orientations and in some cases rounded edges are observed.

Au/commercial ceria showed very small Au particles (2–5 nm, Table 2) found by HAADF (Fig. 4a) and HRTEM (Fig. 4c–e). Au particles are not agglomerated, and are located on the CeO_2 support. The presence of Au was confirmed by EDXS, as displayed in Fig. 4b. FFT (fast Fourier transform) of the image was performed on the labeled squared part of the Au particle in Fig. 4e. A diffraction pattern was obtained, which could be indexed as cubic Au in zone axis [0 −1 1] (Fig. 4f).

Gold nanoparticles (10–20 nm size) are present in the sample prepared at $pK_a = 8.5$, $T = 120\ ^\circ C$ with 1% Au, as can be seen in Fig. 5a and Table 2. Particle size was similar for the sample prepared at $pK_a = 8.5$, at $T = 150\ ^\circ C$ (10–20 nm, Table 2). The particle size is larger when the preparation temperature is 220 °C (20–30 nm, Fig. 5c and Table 2) and even larger for $pK_a = 26.5$ and $T = 150\ ^\circ C$ (20–40 nm, Table 2). It can be seen increasing preparation temperatures and/or pK_a of the ceria supports, causes an increase in the Au particle size deposited on them.

Table 2
Gold particle sizes of Au/ceria samples determined by HRTEM/HAADF.

Ceria support	Au nanoparticle size (nm)
Commercial	2–5
Solvothermal, $pK_a = 8.5$, 120 °C	10–20
Solvothermal, $pK_a = 8.5$, 150 °C	10–20
Solvothermal, $pK_a = 8.5$, 220 °C	20–30
Solvothermal, $pK_a = 26.5$, 150 °C	20–40

EDXS results showed that the ceria was pure and that that chloride and sodium were present on the samples. It also showed that the amount of Au present was ~0.8 wt.%.

3.1.4. XPS

XPS was used to characterise the commercial ceria and a solvothermal sample (prepared at $pK_a = 8.5$ and $T = 120\ ^\circ C$). The two spectra were quite similar, and so only the latter is shown (Fig. 3b). The theoretical basis for all the components of ceria has been reported in the literature [53,60–63]. The complex spectra can be resolved by deconvolution into eight components. The assignment of each component peak is defined in Fig. 3b (where v, v', v'', v''' represent the Ce $3d_{5/2}$ contributions and u, u', u'', u''' represent the Ce $3d_{3/2}$ contributions). For $3d_{5/2}$ of Ce(4+), a mixing of the Ce $3d^9 4f^2 L^{n-2}$ and Ce $3d^9 4f^1 L^{n-1}$ states produces the peaks labeled v and v'', respectively, and the Ce $3d^9 4f^1 L^n$ final state forms the peak v'''. For $3d_{5/2}$ of Ce(3+), the Ce $3d^9 4f^2 L^{n-1}$ and Ce $3d^9 4f^1 L^n$ states correspond to peaks v and v'. For Ce $3d_{3/2}$ level with the u structure, the same assignment can be carried out. A relationship between the area of CeO_2 in the Ce 3d spectra and the % of u''' peak (at ca. 917 eV, which arises from a transition of the $4f''$ final state from the $4f''$ initial state, and is characteristic of CeO_2, since it is absent in pure Ce_2O_3) was established by Shyu et al. [53], from which a semi-quantitative estimation of the relative amount of cerium present as Ce(IV) was made. The obtained values varied between 90% (for the solvothermal sample prepared at $pK_a = 8.5$ and $T = 120\ ^\circ C$) and 98% (for commercial sample).

Fig. 6 shows Au 4f XPS results for solvothermal ceria prepared at $pK_a = 8.5$ and $T = 120\ ^\circ C$ (a) and commercial ceria (b), both loaded with Au. It can be observed that the commercial sample has Au in the reduced form (Au^0), while the solvothermal sample shows a mixture of oxidic gold (Au^{3+}) and a smaller amount of reduced gold (Au^0). These findings are in agreement with the TPR results as it will be seen in Section 3.1.6.

3.1.5. SAED

Fig. 7 shows SAED images of commercial ceria (a) and the solvothermal sample prepared at $pK_a = 8.5$, $T = 120\ ^\circ C$ (b), both loaded with Au. For all samples analysed (Au/ceria), the diffracted spots correspond to CeO_2 phase; however different crystallite sizes were present. Values estimated from transmission electron micrographs agree well with those determined by XRD. Gold was not detected by SAED, possibly because it was below the detection limit. However, using the FFT approach, as above, it was proved that gold was present in the cubic *Fm-3m* crystalline form, with unit cell size of 0.408 nm for Au/solvothermal, $pK_a = 8.5$, 120 °C sample. These results correlate very well with the value determined by XRD on the same sample (0.40679 nm).

3.1.6. TPR

TPR results are shown in Fig. 8a and b, and show the influence of gold on ceria reducibility for the commercial (a) and the solvothermal samples prepared at 120 °C and $pK_a = 8.5$ (b), with and without Au. Two peaks are seen in the TPR spectra of the pure ceria samples, as expected from the literature [13,17,24,25,27,64,65]. The high-temperature peak (~850 °C) corresponds to the reduction of bulk oxygen and the formation of lower oxides of cerium. It is a little smaller in the case of the solvothermal ceria, but the difference is not high (note that figures

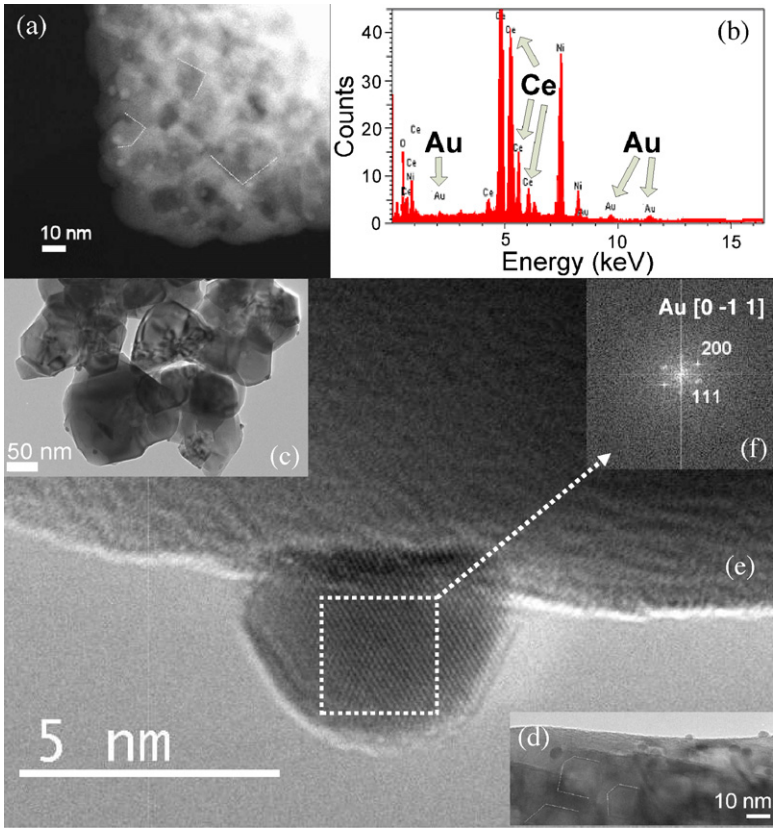

Fig. 4. HAADF image of commercial CeO_2 with 1% Au where gold particles are seen as small bright dots and polygonal features are marked with white dotted lines (a), with respective EDXS spectrum for an average over several grains (b), and HRTEM images of the same sample (c), with polygonal features marked with white dotted lines (d), and a closer detail of a gold particle on the CeO_2 support (e) and the FFT (fast Fourier transform) of the labeled squared part of Au particle obtaining a diffraction pattern of a cubic Au in [0 −1 1] zone axis (f).

a and b have different *y*-scales for better comprehension). The first peak (∼500–600 °C) is assigned to lower temperature ceria surface shell reduction (or reduction of surface oxygen species). It can be observed that this peak is one order of magnitude larger for this solvothermal sample than for the commercial ceria. Other solvothermal samples showed similar peaks, but with a decrease in the intensity with increasing temperature and increasing pK_a (not shown). According to the literature, the size of this first peak appears to be dependent on the method of preparation and on the amount of surface oxygen anions attached to surface Ce^{4+} ions [64]. Therefore, it can be concluded that the amount of surface oxygen is much larger in these samples than in the commercial one. In order to confirm this, we also performed O_2-TPD analysis of these samples. Fig. 8c shows a large O_2 desorption peak for the solvothermal sample prepared at pK_a = 8.5, T = 120 °C (for other solvothermal samples, this peak decreased in intensity with

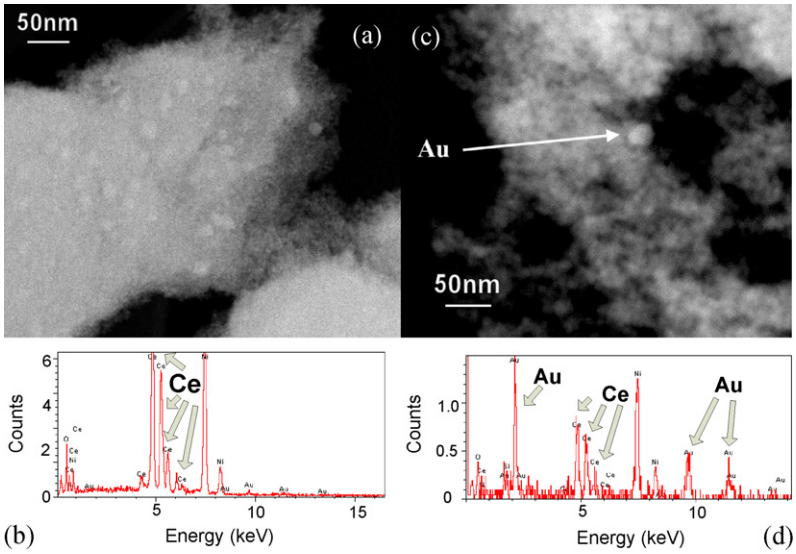

Fig. 5. HAADF images of CeO_2 samples prepared at pK_a = 8.5, T = 120 °C with 1% Au (a) and respective EDXS spectrum collected from an average of CeO_2 grain (b) and prepared at pK_a = 8.5, T = 220 °C with 1% Au (c) and corresponding EDXS spectrum from the Au particle, seen as a bright dot (d).

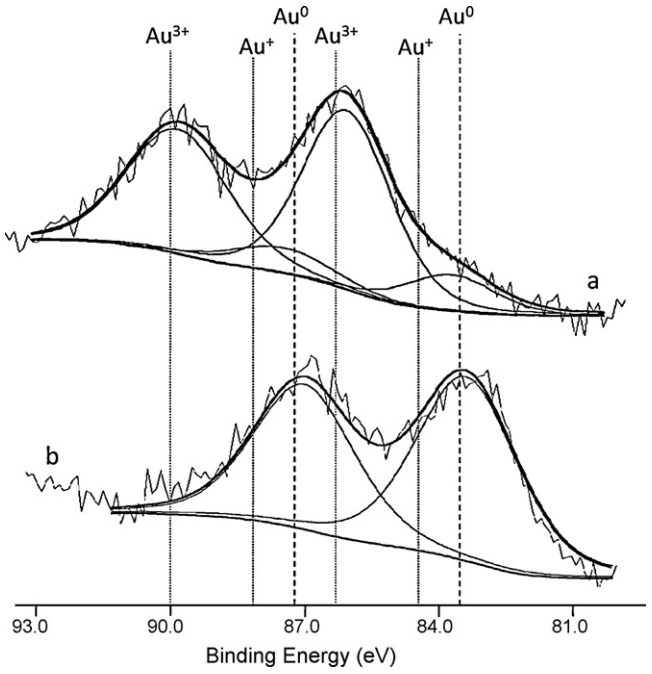

Fig. 6. Au 4f XPS spectra with peak deconvolution of Au on solvothermal ceria prepared at pK_a = 8.5 and T = 120 °C (a) and of Au on commercial ceria (b).

temperature and pK_a increase, confirming the results obtained by TPR), while the peak was one order of magnitude smaller for the commercial sample. The obtained O_2-TPD spectra are similar to what is reported by Behm and co-workers for ceria [31].

According to the literature, when a metal promoter is loaded, the surface shell reduction is facilitated, but usually there is not much effect on the bulk oxygen of ceria [13,17,24,25,27,64,65] (this was also the case in the present work as shown in Fig. 8a and b). In the particular case of Au, the first peak is significantly shifted to lower temperatures (~100 °C, according to the literature, but depending on amount of Au present [13,16,17,24,25,27]), as it can be also observed in the spectra of both ceria samples in Fig. 8a and b. The lowering of the reduction temperature implies that the presence of Au improves the reducibility of the surface oxygen on CeO_2. This facilitates the oxygen transfer across the solid–gas interface during the reaction [13,25]. Such enhanced reduction behaviour has also been observed in the case of other noble metals supported on ceria [64,65].

One single peak, at lower temperatures, is visible in the spectrum for the commercial sample loaded with Au (Fig. 8a) and its area is exactly the same as the area of the corresponding peak of the Au-free sample, indicating that most gold is in the metallic state, as stated by other authors [25]. This was confirmed by XPS (Fig. 6b) as seen in Section 3.1.4. In contrast, two low temperature peaks are visible for the solvothermal sample (Fig. 8b). The first can be attributed to oxygen adsorbed on the surface of metallic gold and the second to reduction of Au(III) [25]. Neri et al. [66] reported two separate peaks (125 and 175 °C) for Au/Fe_2O_3 without calcination. However, after oxidation at 300 °C, only one peak (165 °C) was observed. These authors attributed the first peak to the reduction of Au oxide or hydroxide, which decomposes with calcination above 300 °C, as stated by Haruta et al. [1,67] In fact, it was seen in the present work that when Au was deposited on a calcined solvothermal ceria sample, this peak disappeared from the TPR spectrum (not shown), thus confirming its nature. Since all profiles of the solvothermal samples showed similar results (not shown), that is, more than one peak in the lower temperature region, contribution from oxidic gold reduction is evident, although in some cases it can be masked by the higher amount of ceria–oxygen. The presence of oxidic gold (Au^{3+}) was also confirmed by XPS (Fig. 6a), as seen in Section 3.1.4.

3.2. Catalytic tests

3.2.1. Ceria samples

Fig. 9a shows the CO oxidation results obtained for all pure ceria samples. There is practically no conversion below 200 °C (~5% maximum), and full conversion is only achieved at 400–700 °C. Venezia et al. also obtained full conversion of CO at ~450 °C for pure CeO_2 [13]. The solvothermally prepared ceria is more active than the commercial sample. It can be seen that the best preparative conditions for the CeO_2 particles are pK_a = 8.5 and T = 120 °C. Increasing the temperature produces less active samples, which seems to be related with the decrease in the BET surface area and the increase in the particle size (Table 1). Strangely, an increase in the pK_a (from 8.5 to 26.5, at 150 °C), although causing an increase in the surface area (from 138 to 157 m^2/g, Table 1) and a decrease in the particle size (from 5.74 to 4.57 nm, Table 1), does not produce a more active sample. This can be related with its smaller surface oxygen content, shown to decrease with increasing temperature and increasing pK_a, as discussed in Section 3.1.5. Thus it seems that the activity of the

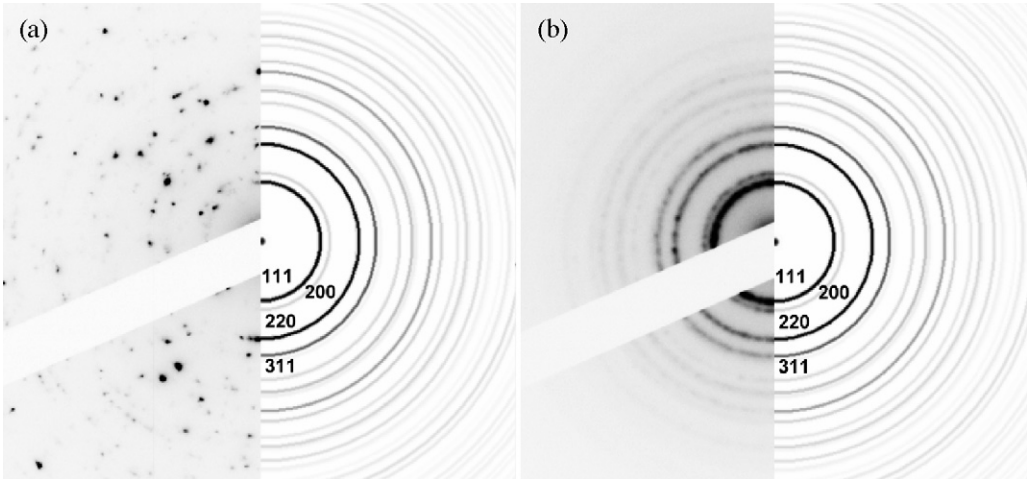

Fig. 7. SAED images of commercial ceria sample (a) and the solvothermal prepared sample at pK_a = 8.5, T = 120 °C (b), both loaded with Au. The right parts of the images are simulated SAED powder diffraction patterns for cubic Au with particle size of 5 nm.

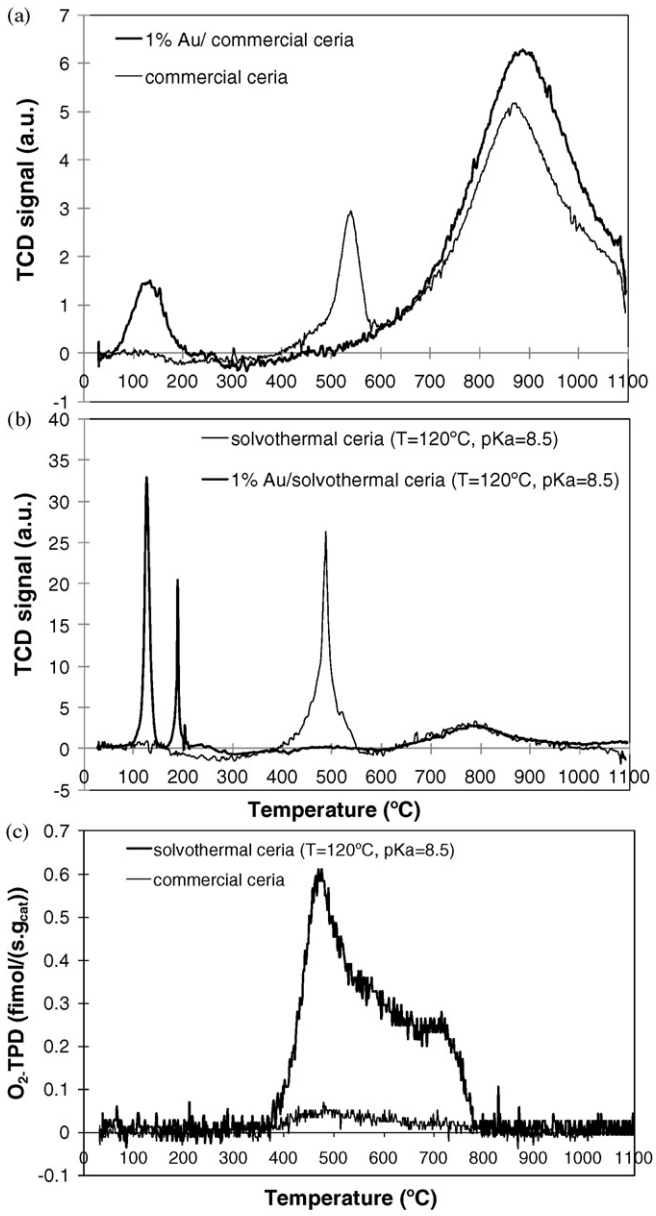

Fig. 8. H_2-TPR profiles of commercial ceria sample (a) and solvothermal prepared sample at pK_a = 8.5, T = 120 °C (b), with and without Au; and O_2-TPD profiles of commercial and solvothermal prepared sample at pK_a = 8.5, T = 120 °C (c).

pure ceria supports is closely related with the surface oxygen content.

3.2.2. Au/ceria catalysts

Loading the samples with Au (Fig. 9b) causes CO total conversion to occur at much lower temperatures than with the supports alone, as expected. For the Au/(solvothermal samples prepared at pK_a = 8.5, T = 120 and 150 °C), the CO conversion is practically complete (above 95%) when the reaction temperature reaches 150 °C. For the sample prepared at the same pK_a, but at T = 220 °C, loaded with Au, near full conversion is achieved at 200 °C. For the pK_a = 26.5, T = 150 °C support with Au, that only happens at 320 °C. The Au supported on commercial ceria (treated and untreated), reached ~95% CO conversion at 110–120 °C. All these materials show better performance than the WGC catalyst, with the exception of the solvothermal ceria sample prepared at pK_a = 26.5, T = 150 °C, which is slightly worse than the reference material up to 200 °C.

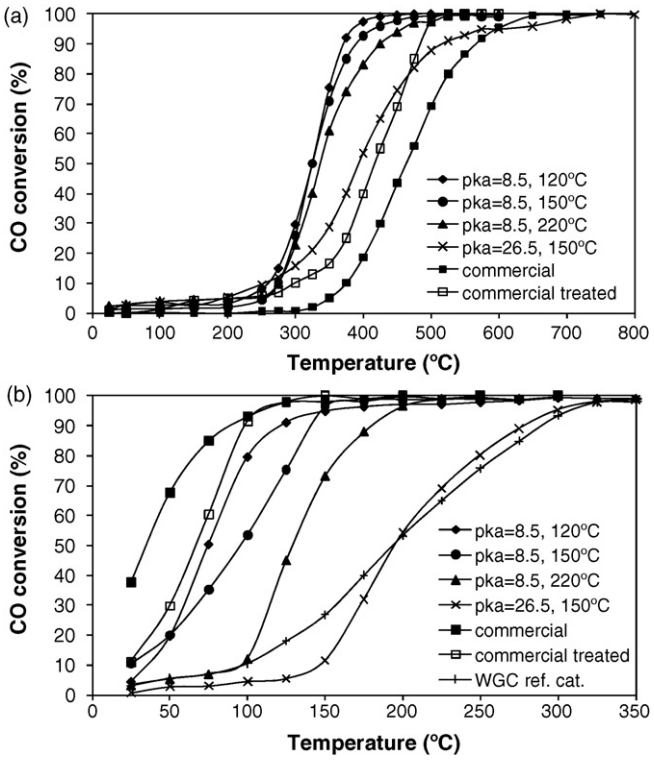

Fig. 9. CO conversion (%) versus temperature for the ceria supports (a) and Au/ceria samples prepared by DIM and the WGC reference catalyst (b).

In order to check for the possible effect of calcination on the solvothermal samples, we also tested the ceria support prepared at pK_a 8.5 and T = 150 °C, calcined at 400 °C and loaded with Au. It was found that the CO conversion results were very similar (not shown), so all other experiments with the other solvothermal samples presented in this paper were carried out with the uncalcined supports for simplicity.

Commercial ceria with Au yielded the best CO conversion results of this set of studies (Fig. 9b). This can be explained by the very small Au particles (2–5 nm, Table 2), well known to be correlated with the particle size [3–11]. Solvothermal supports which showed larger Au nanoparticle sizes (Table 2) are less active. Particle size was similar for the samples prepared at pK_a = 8.5, at T = 120 and 150 °C (10–20 nm, Table 2), which correlates well with the CO conversion results (Fig. 9b). The particle size is larger when the preparation temperature is 220 °C (20–30 nm, Table 2) and even larger for pK_a = 26.5 and T = 150 °C (20–40 nm, Table 2). That explains their lower activities in CO oxidation.

Increasing the pK_a and/or the temperature of preparation, results in less active samples, also when gold is loaded, just like when used as pure catalysts. This can be linked also with the decrease in the surface oxygen content when increasing pK_a and/or preparation temperature, since it is widely accepted that the mechanism for CO oxidation involves the lattice oxygen of the support, as proposed in 2000 by Bond and Thompson [68], and substantiated by subsequent results of several authors [69]. Nevertheless, the commercial sample, in spite of the low oxygen content, when compared with the solvothermal samples, showed to be the best support for gold, yielding the smallest nanoparticles of this study. The reasons for this fact need further investigation.

In spite of the "large" particle size of these solvothermal materials, which is far from the "ideal" range reported in the literature (below 5 nm) [3–11], it is quite interesting that they still show a catalytic behaviour superior to the WGC reference catalyst,

Table 3
Specific rates for CO oxidation for the Au/ceria samples and the Au/Fe_2O_3 reference catalyst at room temperature.

Ceria support	Specific rates ($mol_{CO}\,h^{-1}\,g_{Au}{}^{-1}$)
Solvothermal, pK_a = 8.5, 120 °C	0.17
Solvothermal, pK_a = 8.5, 150 °C	0.41
Solvothermal, pK_a = 8.5, 220 °C	0.13
Solvothermal, pK_a = 26.5, 150 °C	0.03
Commercial	1.46
Commercial treated	0.43
Reference catalyst	0.11

with the exception of the sample prepared at higher pK_a, as seen above (Fig. 9b). As already referred, Corma and co-workers reported that the addition of gold nanoparticles to mesoporous CeO_2 nanocrystals increased the activity for CO oxidation by two orders of magnitude [12]. These results were obtained at 10 °C, but for 0.2% of CO, while we used 5% of this gas (and in the literature the most common is around 1% CO or less [9–14,17–19]). Also most studies also use higher loadings of Au [9–13,15,17,19] (while we used 1 wt.%). Nevertheless, it is possible to see that at room temperature, CO conversion increases from 2 to 10 times (up to 1 order of magnitude) by the addition of Au, when compared to the unloaded ceria samples, while the increase is more than 1000 times (3 orders of magnitude) for the commercial sample.

Comparing with the activities reported in the literature, namely by Corma and co-workers [12] (0.38 $mol_{CO}\,h^{-1}\,g_{Au}{}^{-1}$ for a Au/CeO_2 catalyst and 0.05 $mol_{CO}\,h^{-1}\,g_{Au}{}^{-1}$ for the Au/Fe_2O_3 World Gold Council reference catalyst, at 5 °C), it can be seen that our values, for the solvothermal samples, at room temperature, displayed in Table 3, are within the same order of magnitude, while the value for untreated commercial ceria is higher. Another usual way to express rates in the literature is per mass of catalyst and values ranging from 5.4×10^{-8} to 6×10^{-6} $mol_{CO}\,s^{-1}\,g_{cat}{}^{-1}$ have been reported for Au/ceria catalysts by several authors, using different conditions [12,13,17]. Our values ranging from 6×10^{-8} to 3.2×10^{-6} $mol_{CO}\,s^{-1}\,g_{cat}{}^{-1}$ are also within the same range. Of course, consideration must be taken when comparing since different conditions are used.

It is claimed that the effect of the oxidation state of gold on CO oxidation is very important, and in fact there is a strong controversy about this subject, some authors suggesting that part of the gold is non-metallic, others reporting that oxidised or partially oxidised gold species are the most active sites, while many others suggest that metallic gold is the active species [9,10]. In the particular case of Au/CeO_2 catalysts, some authors suggest that the catalytic sites for CO oxidation are the metal nanoparticles, and not ionic Au [36,18]. In fact, a combined experimental and computational investigation of gold catalysts, which were found to be exceptionally active for the water-gas shift reaction, led to the conclusion that the active form of gold was metallic [70]. The same authors concluded that metallic gold in close contact with the ceria-based support provided the active sites for the water-gas shift reaction on those very active catalysts [70]. These conclusions are very important, since CO oxidation can be considered mechanistically related to the water-gas shift reaction [19]. The results of the present work show that the samples where Au is in its metallic state (Au/commercial ceria) are the most active.

4. Conclusions

Ultrafine cubic shaped CeO_2 particles were prepared by the solvothermal method, which showed better performance as pure supports than the commercial ceria for CO oxidation, possibly due to larger amounts of surface oxygen. However, when gold was loaded on the samples, the best catalytic results were obtained with the commercial sample, which can be explained by the very small gold particles (2–5 nm) found. Samples prepared by the solvothermal method yielded larger Au particle sizes (~10–30 nm), which can explain their lower activity in CO oxidation. Although the gold particle size of the solvothermal samples is far from the "ideal" range (below 5 nm), they still showed, in general, a superior catalytic behaviour in comparison to the reference catalyst. The activity values for the Au/ceria catalysts are within those reported in the literature. It was shown that Au was in its metallic state when supported in the commercial sample, while oxidic Au was mostly present in the Au/solvothermal samples.

Acknowledgments

Authors acknowledge Fundação para a Ciência e Tecnologia (FCT), Portugal, and the Ministry of Higher Education, Science and Technology, from Slovenia, for financial support from the Portugal–Slovenia Cooperation in Science and Technology (2008–2009), project "Synthesis and Characterization of Nanostructured Catalytic Materials". Further support from FCT and FEDER was provided under project REEQ/1106/EQU/2005. SACC and AMTS also acknowledge FCT for financing (CIENCIA 2007 program and POCI/N010/2006 project, respectively). GD acknowledges the financial support of the Slovenian Research Agency.

References

[1] M. Haruta, T. Kobayashi, H. Sano, N. Yamada, Chem. Lett. (1987) 405.
[2] M. Haruta, N. Yamada, T. Kobayashi, S. Iijima, J. Catal. 115 (1989) 301.
[3] G.C. Bond, D.T. Thompson, Catal. Rev. Sci. Eng. 41 (1999) 319.
[4] M. Haruta, M. Daté, Appl. Catal. A 222 (2001) 427.
[5] M. Haruta, Cattech 6 (2002) 102.
[6] M. Haruta, Chem. Rec. 3 (2003) 75.
[7] G.J. Hutchings, Catal. Today 100 (2005) 55.
[8] A.S.K. Hashmi, G.J. Hutchings, Angew. Chem. Int. Ed. 45 (2006) 7896.
[9] G.C. Bond, C. Louis, D.T. Thompson, in: G.J. Hutchings (Ed.), Catalysis by Gold, Imperial College Press, London, 2006, , references cited therein.
[10] S.A.C. Carabineiro, D.T. Thompson, in: U. Heiz, U. Landman (Eds.), Nanocatalysis, Springer-Verlag, Berlin, Heidelberg, New York, 2007, pp. 377–489 (ISBN-13 978-3-540-32645-8) and references cited therein.
[11] S.A.C. Carabineiro, D.T. Thompson, in: C. Corti, R. Holliday (Eds.), Gold: Science and Applications, CRC Press, Taylor and Francis Group, Boca Raton, London, New York, 2010, pp. 89–122 (ISBN-978-1-4200-6523-7) and references cited therein.
[12] S. Carrettin, P. Concepción, A. Corma, J.M.L. Nieto, V.F. Puntes, Angew. Chem. Int. Ed. 43 (2004) 2538.
[13] A.M. Venezia, G. Pantaleo, A. Longo, G. Di Carlo, M. Casaletto, F.L. Liotta, G. Deganello, J. Phys. Chem. B 109 (2005) 2821.
[14] P.X. Huang, F. Wu, B.L. Zhu, X.P. Gao, H.Y. Zhu, T.Y. Yan, W.P. Huang, S.H. Wu, D.Y. Song, J. Phys. Chem. B 109 (2005) 19169.
[15] D. Widmann, R. Leppelt, R.J. Behm, J. Catal. 251 (2007) 437.
[16] U.R. Pillai, S. Deevi, Appl. Catal. A 299 (2006) 266.
[17] S.-Y. Lai, Y. Qiu, S. Wang, J. Catal. 237 (2006) 303.
[18] N. Hickey, P.A. Larochette, C. Gentilini, L. Sordelli, L. Olivi, S. Polizzi, T. Montini, P. Fornasiero, L. Pasquato, M. Graziani, Chem. Mater. 19 (2007) 650.
[19] Z.R. Tang, J.K. Edwards, J.K. Bartley, S.H. Taylor, A.F. Carley, A.A. Herzing, G.J. Hutchings, J. Catal. 249 (2007) 208.
[20] Z. Chen, Q. Gao, Appl. Catal. B 84 (2008) 790.
[21] V. Aguilar-Guerrero, B.C. Gates, J. Catal. 260 (2008) 351.
[22] F. Romero-Sarria, A. Penkova, L.M. Martinez, M.A. Centeno, K. Hadjivanov, J.A. Odriozola, Appl. Catal. B 84 (2008) 119.
[23] V. Aguilar-Guerrero, R.J. Lobo-Lapidus, B.C. Gates, J. Phys. Chem. C 113 (2009) 3259.
[24] D. Andreeva, V. Idakiev, T. Tabakova, L. Ilieva, P. Falaras, A. Bourlinos, A. Travlos, Catal. Today 72 (2002) 51.
[25] Q. Fu, S. Kudriavtseva, H. Saltsburg, M. Flytzani-Stephanopoulos, Chem. Eng. J. 93 (2003) 41.
[26] H. Sakurai, T. Akita, S. Tsubota, M. Kiuchi, M. Haruta, Appl. Catal. A 291 (2005) 179.
[27] Q. Fu, W. Deng, H. Saltsburg, M. Flytzani-Stephanopoulos, Appl. Catal. B 56 (2005) 57.
[28] C.H. Kim, L.T. Thompson, J. Catal. 230 (2005) 66.
[29] G. Jacobs, S. Ricote, B.H. Davis, Appl. Catal. A 302 (2006) 14.
[30] A. Karpenko, R. Leppelt, V. Plzak, J. Cai, A. Chuvilin, B. Schumacher, U. Kaiser, R.J. Behm, Top. Catal. 44 (2007) 183.
[31] A. Karpenko, Y. Denkwitz, V. Plzak, J. Cai, R. Leppelt, B. Schumacher, R.J. Behm, Catal. Lett. 116 (2007) 105.
[32] Z.-Y. Yuan, V. Idakiev, A. Vantomme, T. Tabakova, T.-Z. Ren, B.-L. Su, Catal. Today 131 (2008) 203.
[33] A. Luengnaruemitchai, S. Osuwan, E. Gulari, Int. J. Hydrogen Energy 29 (2004) 429.

[34] F. Arena, P. Famulari, G. Trunfio, G. Bonura, F. Frusteri, L. Spadaro, Appl. Catal. B 66 (2006) 81.
[35] G. Avgouropoulos, M. Manzoli, F. Boccuzzi, T. Tabakova, J. Papavasilou, T. Ioannides, V. Idakiev, J. Catal. 256 (2008) 237.
[36] M. Manzoli, G. Avgouropoulos, T. Tabakova, J. Papavasiliou, T. Ionnides, F. Boccuzzi, Catal. Today 138 (2008) 239.
[37] X.D. Zhou, W. Huebner, H.U. Anderson, Appl. Phys. Lett. 80 (2002) 3814.
[38] J. Zhu, Q. Gao, Z. Chen, Appl. Catal. B 81 (2008) 236.
[39] Y. Zhang, R. Si, C. Liao, C. Yan, C. Xiao, Y. Kou, J. Phys. Chem. B 107 (2003) 10159.
[40] H. Chen, H. Chang, Solid State Commun. 133 (2005) 593.
[41] W. Han, L. Wu, Y. Zhu, J. Am. Chem. Soc. 127 (2005) 12814.
[42] T. Yu, J. Joo, Y.I. Park, T. Hyeon, Angew. Chem. Int. Ed. 44 (2005) 7411.
[43] A.I.Y. Tok, F.Y.C. Boey, Z. Dong, X.L. Sun, J. Mater. Process. Technol. 190 (2007) 217.
[44] J.-S. Lee, S.-C. Choi, Mater. Lett. 58 (2004) 390.
[45] E. Verdon, M. Devalette, G. Demazeau, Mater. Lett. 25 (1995) 127.
[46] X. Zheng, S. Wang, X. Wang, S. Wang, X. Wang, S. Wu, Mater. Lett. 59 (2005) 2769.
[47] T. Kobayashi, S. Iwamoto, M. Inoue, J. Alloys Compd. 408–412 (2006) 1149.
[48] A.M.T. Silva, B.F. Machado, H.T. Gomes, J.L. Figueiredo, G. Drazic, J.L. Faria, J. Nanopart. Res. 12 (2010) 121.
[49] M. Bowker, A. Nuhu, J. Soares, Catal. Today 122 (2007) 245.
[50] See http://www.utilisegold.com/uses_applications/catalysis/reference_catalysts/ (World Gold Council Catalysts website).
[51] W. Kraus, G. Nolze, PowderCell for Windows, version 2.3, available at http://www.ccp14.ac.uk/tutorial/powdcell/.
[52] K.A. Thomas, P.S.I.P.N. de Silva, L.F. Cohen, A. Hossain, M. Rajeswari, T. Venkatesan, R. Hiskes, J.L. MacManus-Driscoll, J. Appl. Phys. 84 (1998) 3939.
[53] J.Z. Shyu, K. Otto, W.L.H. Watkins, G.W. Graham, R.K. Belitz, H.S. Gandhi, J. Catal. 114 (1988) 23.
[54] S.C. Lada, R. Ryoo, Chem. Commun. (2003) 2138.
[55] M. Manzoli, A. Chiorino, F. Boccuzzi, Stud. Surf. Sci. Catal. 155 (2005) 405.
[56] M. Sakurai, S. Tsubota, M. Haruta, Appl. Catal. A 102 (1993) 125.
[57] F. Moreau, G.C. Bond, B. van der Linden, B.A.A. Silberova, M. Makkee, Appl. Catal. A 347 (2008) 208.
[58] A.I.Y. Tok, F.Y.C. Boey, Z. Dong, X.L. Sung, J. Mater. Process. Technol. 190 (2007) 217.
[59] A. Sepulveda-Escribano, F. Coloma, F. Rodriguez-Reinoso, J. Catal. 178 (1998) 649.
[60] C. Pan, D. Zhang, L. Shi, J. Fang, Eur. J. Inorg. Chem. (2008) 2429.
[61] C. Sun, H. Li, L. Chen, J. Phys. Chem. Solids 68 (2007) 1785.
[62] S. Tsunekawa, T. Fukuda, A. Kasuya, Surf. Sci. 457 (2000) L437.
[63] V. Matolín, I. Matolínová, L. Sedláček, K.C. Prince, T. Skála, Nanotechnology 20 (2009) 215706.
[64] B. Harrison, A.F. Diwell, C. Hallett, Platinum Met. Rev. 32 (1988) 73.
[65] G. Jacobs, E. Chenu, P.M. Patterson, L. Williams, D. Sparks, G. Thomas, B.H. Davis, Appl. Catal. A 258 (2004) 203.
[66] G. Neri, A.M. Visco, S. Galvagno, A. Donato, M. Panzalorto, Therm. Acta 329 (1999) 39.
[67] M. Haruta, S. Tsubota, T. Kobayashi, J. Kageyama, M.J. Genet, B. Delmon, J. Catal. 144 (1993) 175.
[68] G.C. Bond, D.T. Thompson, Gold Bull. 33 (2000) 41.
[69] G.C. Bond, D.T. Thompson, Gold Bull. 42 (2009) 247.
[70] D. Tibiletti, A. Amieiro-Fonseca, R. Burch, Y. Chen, J.M. Fisher, A. Goguet, C. Hardacre, P. Hu, D. Thompsett, J. Phys. Chem. B 109 (2005) 22553.